ADVANCED ENGINEERING MATERIALS
www.aem-journal.com

Phosphorous Catalytic-Doping of Silicon Alloys for the Use in Silicon Heterojunction Solar Cells

*Yong Liu, Manuel Pomaska, Weiyuan Duan, Do Yun Kim, Malte Köhler, Uwe Breuer, and Kaining Ding**

Herein, the effectiveness of post-deposition catalytic-doping (cat-doping) on various doped silicon alloys, i.e., microcrystalline silicon (μc-Si:H), nanocrystalline silicon oxide (nc-SiOx:H), and microcrystalline silicon carbide (μc-SiC:H), for the use in silicon heterojunction solar cells is investigated. Phosphorous (P) profiles by secondary ion mass spectrometry (SIMS) reveal the P distribution and its difference in these three silicon alloy films. Conductivity and effective charge carrier lifetime of different samples are found to increase to different extents after cat-doping process. Coexistence of thermal annealing, hydrogenation, and phosphorus doping is confirmed by using different gases during the cat-doping process.

1. Introduction

Among many innovative solar cell techniques, silicon heterojunction (SHJ) solar cells are one of the most promising candidates for the next-generation high-efficiency mainstream photovoltaic technology due to their high efficiencies and simple production sequences.[1] In a SHJ solar cell, an intrinsic hydrogenated amorphous silicon (a-Si:H(i)) thin film is usually used to achieve an excellent surface passivation quality. Doped a-Si:H layers are used as emitter or surface field layer.[1–4] SHJ solar cell efficiency over 23% has been achieved for mass production.[5] However, there is still optical loss from the parasitic absorption in the solar spectrum range due to the use of doped a-Si:H layers at the front side[1,6] as well as loss from the lower conductive a-Si:H layers. Silicon alloy thin-films, such as microcrystalline silicon (μc-Si:H), nanocrystalline silicon oxide (nc-SiO_x:H), and microcrystalline silicon carbide (μc-SiC:H),[7–9] are very promising alternatives to be used in a SHJ solar cell to reduce the contact resistance and parasitic absorption due to their higher conductivity and lower absorption coefficient in short wavelength range.

In addition to the implementation of silicon alloys, catalytic-doping (cat-doping) has the potential to further improve electrical properties of the films and the interfaces. Cat-doping is a cheap, simple, and up-scalable post-deposition treatment, which is based on the hot-wire chemical vapor deposition (HWCVD) technique. During a cat-doping process, the gas molecules decompose at the hot surface of the catalyzing wires, then the decomposed radicals diffuse radially toward the sample and penetrate into the surface of the silicon films forming a shallow depth doping layer with a thickness of 5–15 nm.[10,11] With cat-doping, material properties, e.g., conductivity and doping concentration, can be tuned beyond the level which is achievable for as-grown films.[11,12] Especially for materials, where the conductivity is limited upward due to restrictions from process boundary conditions during film depositions or from trade-off with other device relevant material properties, the cat-doping process might be beneficial to overcome the limit or find better trade-off regime.

So far, cat-doping has been studied mainly on crystalline silicon, amorphous silicon, and microcrystalline silicon.[10,11,13,14] Former studies have shown that cat-doping can improve the conductivity of a-Si:H and μc-Si:H films. Cat-doping can also improve the passivation quality of the passivated samples with symmetric structures of μc-Si:H(n)/a-Si:H(i)/c-Si/a-Si:H(i)/μc-Si:H(n) and a-Si:H(n)/a-Si:H(i)/c-Si/a-Si:H(i)/a-Si:H(n) in which the interfaces of μc-Si:H(n) and c-Si are cat-doped, respectively.[10,14–16]

In this work, we investigate the phosphorus cat-doping on μc-Si:H(n), nc-SiO_x:H(n), and μc-SiC:H(n) for the use in SHJ solar cells. The phosphorus distribution profiles of three silicon alloy films after cat-doping process were obtained by secondary ion mass spectrometry (SIMS).The impact of cat-doping on

Y. Liu, Dr. M. Pomaska, Dr. W. Duan, M. Köhler, Dr. K. Ding
IEK-5 Photovoltaics
Forschungszentrum Jülich, Wilhelm-Johnen-Strasse
52425 Jülich, Germany
E-mail: k.ding@fz-juelich.de

Dr. U. Breuer
Central Institute for Engineering
Electronics and Analytics (ZEA-3)
Forschungszentrum Jülich, Wilhelm-Johnen-Strasse
52425 Jülich, Germany

Dr. D. Y. Kim
Device Solution Division
Samsung Electronics Semiconductor R&D Center
1, Samsungjeonja-ro, Hwaseong-si, Gyeonggi-do 18448, South Korea

The ORCID identification number(s) for the author(s) of this article can be found under https://doi.org/10.1002/adem.201900613.

DOI: 10.1002/adem.201900613

electrical property of silicon alloy films was evaluated from conductivity measurement. Symmetric passivated samples consisting of the three aforementioned silicon alloys were fabricated for comparison of the enhancement of passivation quality due to application of cat-doping. Different gases were used to reveal coexistence of three effects, i.e., thermal annealing, hydrogenation, and phosphorus (P) doping, during the cat-doping process.

2. Results

First, SIMS was used to investigate the distribution of P atoms after cat-doping process in three silicon alloy films (phosphorus-doped n-type μc-Si:H and nc-SiO_x:H and nitrogen-doped n-type μc-SiC:H). For comparison, reference samples without cat-doping were also included. The SIMS results for samples with and without cat-doping are shown in **Figure 1**. Sketches of the SIMS samples with three silicon alloys are also illustrated in Figure 1 where the color gradient indicates that the cat-doping was done at the interface of silicon alloy films and capping layer. For μc-Si:H(n) with cat-doping, as shown in Figure 1a, there is an increase in the P atoms concentration from $3{\cdot}10^{20}$ to $6{\cdot}10^{20}$ cm^{-3} at the interface of a-Si:H(i) capping layer and the μc-Si:H(n) layer. The penetration depth of P atoms from cat-doping is ≈5 nm from the interface into the μc-Si:H(n) layer. For nc-SiO_x:H(n) in Figure 1b, there is also an increase in P atoms concentration from $2{\cdot}10^{20}$ to $3.5{\cdot}10^{20}$ cm^{-3} throughout the 20 nm nc-SiO_x:H(n) film. For μc-SiC:H(n) in Figure 1c, there is barely any increase of P atoms concentration in the film and the P atoms seem to attach only to the surface of μc-SiC:H(n) film with a concentration of 6×10^{19} cm^{-3}. It should be noted that the μc-SiC:H(n) thin film is initially nitrogen doped, so no P atoms exist in the reference sample. SIMS measurements of multiple samples are included as dash lines in Figure 1 to confirm the difference in P atoms concentration, and the black curve in Figure 1c indicates the detect limit of SIMS.

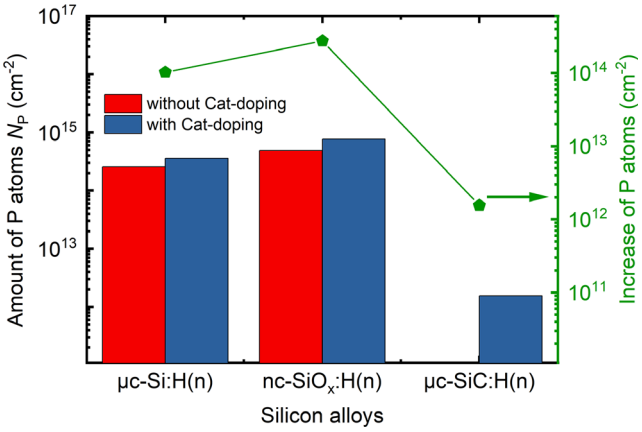

Figure 2. Amount of P atoms and increase after cat-doping for three silicon alloys.

The amount of P atoms per unit area (cm^{-2}) is derived by integrating throughout the cat-doped films and the increase of P atoms per unit area after cat-doping is then calculated for comparison. As shown in **Figure 2**, the amount of P atoms in the silicon alloy films all increased after cat-doping, but with different numbers. The increase of P atoms for μc-Si:H(n) and nc-SiOx:H(n) after cat-doping is 1×10^{14} and 2.7×10^{14} cm^{-2}, respectively. For μc-SiC:H(n), the increase of P atoms is 2 orders of magnitude less, only 1.6×10^{12} cm^{-2}.

The impact of the cat-doping on the electrical properties of silicon alloy films is evaluated by measuring the conductivity of the three different silicon alloy samples before and after the P cat-doping process on the same samples. The results are shown in **Figure 3**. Since the conductivity changes for μc-Si:H(n) and

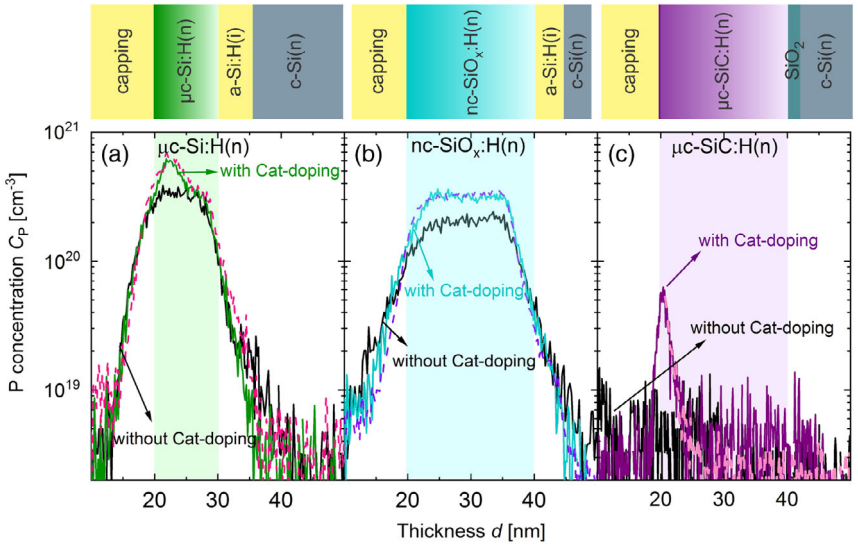

Figure 1. Sketches of SIMS samples with three silicon alloys and P atoms distribution in three silicon alloys with and without cat-doping by SIMS. P profiles for μc-Si:H(n), nc-SiOx:H(n) and μc-SiC:H(n) are shown in (a), (b) and (c), respectively. In graph (a), (b) and (c), the black curves represent P profiles for reference samples without cat-doping; the colored curves represent P profiles for samples with cat-doping and the colored dash curves represent P profiles from repetition of each material.

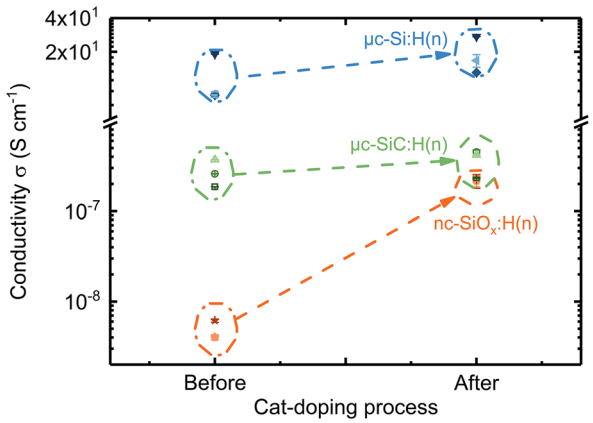

Figure 3. Electrical conductivity of silicon alloy films before and after P cat-doping.

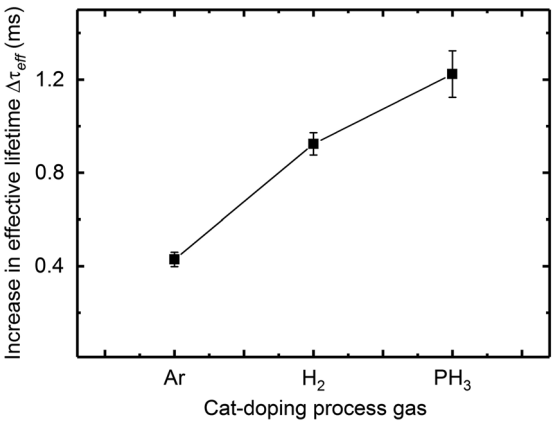

Figure 5. Increase in effective lifetime with different cat-doping process gases.

μc-SiC:H(n) are within the measurement error, multiple samples were measured to confirm the increase in conductivity. The average conductivity of all three silicon alloys increased after the same P cat-doping process—however to different extents. For μc-Si:H(n), the average conductivity increases from 12 to 19 S cm^{-1}. In comparison, the average conductivity of the μc-SiC:H(n) samples just increases slightly from $3{\cdot}10^{-7}$ to $4{\cdot}10^{-7}$ S cm^{-1}. The average conductivity of the nc-SiO$_x$:H(n) samples increased largely by 2 orders of magnitude from 4×10^{-9} to 2×10^{-7} S cm^{-1}.

Passivated samples (*S*1, *S*2, and *S*3) were also fabricated for comparison of effective lifetime change before and after P cat-doping. The P cat-doping process was carried out on both sides of the samples on the surfaces of the silicon alloys. Effective lifetimes of all the samples were measured before and after P cat-doping, as shown in **Figure 4**. The τ_{eff} of *S*1 increases from 3.4 to 4.6 ms after P cat-doping. The τ_{eff} of *S*2 and *S*3 before cat-doping are 1.1 and 2.1 ms, respectively. After cat-doping, the τ_{eff} of *S*2 and *S*3 remain unchanged.

Three effects may coexist during the cat-doping process: thermal annealing effect, hydrogenation, and phosphorous doping. The significance of three aforementioned effects was distinguished by using three different gases, i.e., Ar, H_2, and PH_3, during the cat-doping process. Samples with the same structure as *S*1 were used. The increase in τ_{eff} is shown in **Figure 5**. The τ_{eff} increases by 0.4 and 0.9 ms, respectively, when Ar and H_2 were used. The largest τ_{eff} increase of 1.2 ms was achieved when PH_3 was used.

3. Discussion

First of all, the SIMS results are shown in Figure 1, the profiles of the P concentration arising by cat-doping are different in the three silicon alloy films. The P atoms penetrate into μc-Si:H(n) films for ≈5 nm from the interface of capping layer and μc-Si:H(n) layer, and for nc-SiO$_x$:H(n), the P atoms were incorporated throughout the 20 nm film. However, for μc-SiC:H, there is only small amount of P atoms that was detected at the surface of the film. The SIMS results show that the incorporation of P atoms into films is different in the three silicon alloy films. In the work of Matsumura et al.,[10,11] it was already shown that from cat-doping, P atoms have larger doping depth in a-Si:H than that in c-Si. The different profiles of three silicon alloys might also come from the different microstructures and compositions of these three silicon alloys. However, the correlation between effectiveness of cat-doping and microstructure of the material is yet

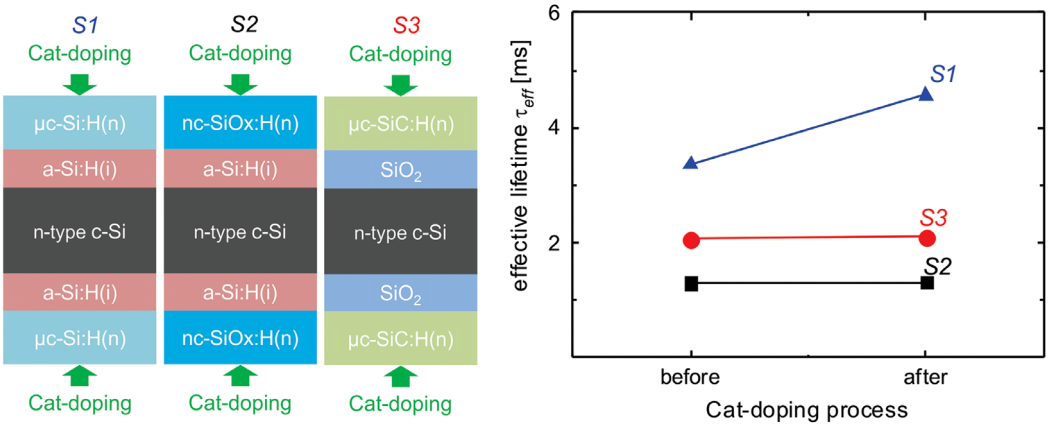

Figure 4. Sketch of passivated samples with silicon alloys and effective lifetime before and after P cat-doping.

not clear. Figure 2 shows the amount of P atoms in all the films evaluated by integrating P profiles with the film thickness. The increase of P atoms after cat-doping is also calculated. For μc-Si:H(n) and nc-SiOx:H(n), a similar increase of P atoms in the order of $10^{14}\,cm^{-2}$ is derived, but for μc-SiC:H(n), the increase of P atoms is two orders of magnitude less, just $1.6 \times 10^{12}\,cm^{-2}$.

As P atoms are known dopant for all three types of silicon alloys,[8,17–19] the electrical conductivity is likely to be increased due to the increase of P atoms concentration. Thus, the electrical conductivity of these films was measured before and after the cat-doping process and the results are shown in Figure 3. The results show that the average conductivity for all sample pieces with different silicon alloy films increased after cat-doping due to incorporation of P atoms, but to a different extent. The μc-Si:H(n) film samples have the largest increase in average conductivity in absolute numbers, in the order of $10^{1}\,S\,cm^{-1}$. For the nc-SiO_x:H(n) samples, the conductivity increased almost by two orders of magnitude, from 10^{-9} to $10^{-7}\,S\,cm^{-1}$. Also for μc-SiC:H(n), the conductivity only increases slightly by $1 \times 10^{-7}\,S\,cm^{-1}$. The reason for the increase in conductivity could be due to the decrease of defect and the increase of mobility and dopants' activation ratio of silicon alloys when the samples are annealed by the hot wires during the cat-doping treatment, which then leads to increase in conductivity.[20,21] Another reason is attributed to the increase in phosphorous donors. However, for μc-Si:H(n) and nc-SiO_x:H(n), the amounts of P atoms incorporated into the films are within the same order of $10^{14}\,cm^{-2}$, the absolute increase in conductivity is much lower for nc-SiO_x:H(n) indicating a much lower doping efficiency of incorporated P atoms. The crystalline volume fraction of μc-Si:H(n) and nc-SiO_x:H(n) was derived from Raman spectrum to be ≈60% and ≈9%, respectively. The lower doping efficiency is partially attributed to a lower crystalline volume fraction as lower doping efficiency has been reported for materials with lower crystalline volume fraction.[22,23] However, the determination of the fraction between active and inactive cat-doped P atoms is still under investigation. For μc-SiC:H(n), the effect of the P atoms at the film surface remains unclear, as not only the doping is very small and superficial but also because the average increase in conductivity of $1 \times 10^{-7}\,S\,cm^{-1}$ is within the error range of the measurement. To increase the conductivity significantly in future, the cat-doping process needs to be adapted to implement more P atoms into μc-SiC:H(n) films that in addition also diffuse deeper into the bulk.

The impact of cat-doping on passivation quality is shown in Figure 4. The τ_{eff} for *S*1 increased by 1.2 ms after cat-doping process, whereas the τ_{eff} stayed the same for *S*2 and *S*3. During the cat-doping process, three effects may coexist. Thermal annealing effect, hydrogenation, and phosphorous doping were already introduced in a former work[15] to play an important role during the cat-doping treatment.

Different cat-doping gases (Ar, H_2, and PH_3) were used to compare the aforementioned three effects and the increase in τ_{eff} is shown in Figure 5. Passivated samples with μc-Si:H(n) were used because it is the only one which shows significant improvement in τ_{eff}. Using Ar atmosphere, we assume similar heat convection inside the HWCVD chamber than during the actual cat-doping treatment, but without the effects from hydrogen radicals and phosphorous dopants. Therefore, the increase of 0.4 ms in τ_{eff} is attributed to the thermal impact of cat-doping treatment and represents 33% of the total increase in τ_{eff} of 1.2 ms. Using a H_2 atmosphere, the thermal effect and hydrogenation effect are combined. Consequently, since the treatment increases τ_{eff} by 0.9, 0.5 ms of the increase should arise from the effect of hydrogenation. Using PH_3 atmosphere finally resulted in the highest increase of 1.2 ms in τ_{eff} where all three aforementioned effects are combined. However, it is not possible to clearly derive the portions of all three effects for the treatment with atmosphere of 2.25% PH_3 in He. Annealing might have a major effect, increasing τ_{eff} in the range of one-third, but the portions of hydrogenation, arising from hydrogen radicals, and increased doping, arising from phosphorous radicals, remain unknown. Nevertheless, the use of PH_3 showed the highest improvement of τ_{eff} with an increase of 1.2 ms. This result confirmed that, with the use of PH_3 gas, all three effects coexist and account for the improvement in τ_{eff}.

4. Conclusions

Phosphorous cat-doping was applied to three different silicon alloys. The results show that phosphorous atoms were incorporated into μc-Si:H(n), nc-SiO_x:H(n), and μc-SiC:H(n) but with different significance in terms of doping depth and conductivity. Thus, with cat-doping, electrical conductivity of μc-Si:H(n), nc-SiO_x:H(n), and μc-SiC:H(n) was increased. Applying different cat-doping treatments on silicon wafers passivated by n-layer/i-layer, strong indication for the convolution of thermal effect, hydrogenation effect, and doping effect was confirmed. Cat-doping might become more important to tune the properties of interfaces for high-efficiency SHJ cells that cannot be improved otherwise.

5. Experimental Section

The μc-Si:H(n) films were deposited by plasma-enhanced chemical vapor deposition (PECVD) using a very high frequency (VHF, 81.36 MHz) generator, the heater temperature was set to 220 °C, a gas mixture of SiH_4, H_2, and PH_3 (diluted in SiH_4) was used, the pressure was 100 Pa; the distance from the 211 cm^2 electrode to the substrate was set to 11 mm and the plasma power was 10 W. More experimental details can be found in previous study.[15] The nc-SiO_x:H(n) films were also deposited by PECVD but with a radio frequency (RF, 13.56 MHz) generator, the heater temperature was set to 200 °C, the pressure was 50 Pa using a gas mixture of SiH_4, H_2, CO_2, and PH_3, the distance from the electrode to the substrate was 16 mm and the plasma power density was around $200\,mW cm^{-2}$, more details on deposition parameters can be found in previous study.[24] The μc-SiC:H(n) films were deposited by HWCVD system using H_2 diluted monomethylsilane (MMS), three curved rhenium filaments were used at a temperature of 1800 °C, the heater temperature was set to 250 °C and pressure was kept at 75 Pa, more details have been published in previous study.[9] It should be noticed that the μc-Si:H(n) and nc-SiO_x:H(n) thin films are initially phosphorus doped during PECVD process and the μc-SiC:H(n) is initially nitrogen doped during HWCVD process.

For the P cat-doping process, phosphine (PH_3, 2.25% diluted by Helium) gas was used with a constant flow rate of 20 sccm. Three winded tantalum filaments in parallel were used with a distance of 20 mm between substrate and filaments. The filament temperature was set to 1000 °C and the heater temperature was 200 °C; the pressure was 1 Pa and the process time was 10 min.

P atoms concentration profiles were measured from the front side by time of flight SIMS (ToF SIMS). For SIMS measurements, the samples are illustrated in Figure 1 and have the following device relevant structures:

15 nm a-Si:H(i)/10 nm μc-Si:H(n)/5 nm a-Si:H(i)/c-Si(n) for μc-Si:H(n), 15 nm a-Si:H(i)/20 nm nc-SiO_x:H(n)/5 nm a-Si:H(i)/c-Si(n) for nc-SiO_x:H(n) and 15 nm a-Si:H(i)/20 nm μc-SiC:H(n)/1.5 nm SiO_2/c-Si(n) for μc-SiC:H(n). Cat-doping processes were carried out at the surface of silicon alloy films. The 15 nm a-Si:H(i) was deposited by PECVD after cat-doping processes as capping layer on top of the silicon alloys films. This capping layer acts as a diffusion barrier for sputter ions and buffer layer when the etch sputter plasma is not stable yet at the beginning of SIMS measurement.

Three different silicon alloys were prepared on glass substrates (Corning EAGLE XG) for conductivity measurements. The conductivity was measured using evaporated silver co-planar contacts in vacuum. After the initial conductivity measurement, the as-grown samples were then processed in a HWCVD chamber for P cat-doping. The conductivity was measured again on the same samples after cat-doping process.

To check the impact of silicon alloys on passivation quality, three different passivated samples were fabricated using n-type double side polished (DSP) float zone wafers (n <111>, with resistivity of 3 Ω cm and thickness of 280 μm). The wafers are RCA (Radio Corporation of America) cleaned before shipment. Before the deposition of μc-Si:H(n) and nc-SiO_x:H(n) films, hydrofluoric (HF) dip was performed to remove native oxide. Then intrinsic amorphous silicon (a-Si:H(i)) layers were deposited on both sides as passivation layers, followed by μc-Si:H(n) and nc-SiO_x:H(n) depositions, respectively. Therefore, they have structures of 10 nm μc-Si:H(n)/5 nm a-Si:H(i)/c-Si(n)/5 nm a-Si:H(i)/10 nm μc-Si:H(n) and 20 nm nc-SiO_x:H(n)/8 nm a-Si:H(i)/c-Si(n)/8 nm a-Si:H(i)/20 nm nc-SiO_x:H(n), hereafter referred to *S*1 and *S*2, respectively. For μc-SiC:H(n), after HF dipped, the wafers were dipped into HNO_3 at 23 °C for 10 min for the formation of a thin SiO_2 layer with a thickness of ≈1.5 nm, where the thin SiO_2 layer is used to passivate the c-Si surface.[25] The passivated samples for μc-SiC:H(n) have a structure of 23 nm μc-SiC:H(n)/1.5 nm SiO_2/c-Si(n)/1.5 nm SiO_2/23 nm μc-SiC:H(n), hereafter referred to *S*3. Cat-doping processes were performed on both sides of *S*1, *S*2, and *S*3. For comparison of different effects during cat-doping, argon (Ar), hydrogen (H_2), and PH_3 are used for cat-doping on *S*1 samples. Minority carrier lifetimes were measured by a Sinton WTC-120 Photoconductance Lifetime Tester, where the effective lifetime (τ_{eff}) was determined at an injection level of 1×10^{15} cm^{-3}.

Acknowledgements

The authors acknowledge Manuela Meyer, Silke Lynen, and Alain Doumit for the help with the experiments, Uwe Zastrow for analyze of SIMS data. The authors also thank Prof. Matsumura for the fruitful discussion on cat-doping. The work is supported by China Scholarship Council (CSC) and has received funding from the European Union's Horizon2020 Programme for research, technological development, and demonstration under Grant Agreement no. 727523. Part of this research was supported by the Helmholtz Energy Materials Foundry (HEMF).

Conflict of Interest

The authors declare no conflict of interest.

Keywords

catalytic chemical vapor deposition, hot-wire chemical vapor depositions, post-depositions, silicon alloy, silicon heterojunction solar cells

Received: May 22, 2019
Revised: August 29, 2019
Published online: September 25, 2019

[1] S. De Wolf, A. Descoeudres, Z. C. Holman, C. Ballif, *Green* **2012**, *2*, 7.
[2] K. Masuko, M. Shigematsu, T. Hashiguchi, D. Fujishima, M. Kai, N. Yoshimura, T. Yamaguchi, Y. Ichihashi, T. Mishima, N. Matsubara, T. Yamanishi, T. Takahama, M. Taguchi, E. Maruyama, S. Okamoto, *IEEE J. Photovoltaics* **2014**, *4*, 1433.
[3] M. Taguchi, A. Yano, S. Tohoda, K. Matsuyama, Y. Nakamura, T. Nishiwaki, K. Fujita, E. Maruyama, *IEEE J. Photovoltaics* **2014**, *4*, 96.
[4] C. Battaglia, A. Cuevas, S. De Wolf, *Energy Environ. Sci.* **2016**, *9*, 1552.
[5] B. Legradic, B. Strahm, D. Lachenal, D. Bätzner, W. Frammelsberger, J. Meixenberger, P. Papet, G. Wahli, Z. Jun, D. Decker, E. Vetter, presented at 2015 IEEE 42nd Photovoltaic Specialist Conf. (PVSC), New Orleans, Louisiana, June 2015.
[6] Z. C. Holman, A. Descoeudres, L. Barraud, F. Z. Fernandez, J. P. Seif, S. De Wolf, C. Ballif, *IEEE J. Photovoltaics* **2012**, *2*, 7.
[7] M. W. M. V. Cleef, J. K. Rath, F. A. Rubinelli, C. H. M. V. D. Werf, R. E. I. Schropp, W. F. V. D. Weg, *J. Appl. Phys.* **1997**, *82*, 6089.
[8] A. Richter, V. Smirnov, A. Lambertz, K. Nomoto, K. Welter, K. Ding, *Sol. Energy Mater. Sol. Cells* **2018**, *174*, 196.
[9] M. Pomaska, A. Richter, F. Lentz, T. Niermann, F. Finger, U. Rau, K. Ding, *Jpn. J. Appl. Phys.* **2017**, *56*, 002302.
[10] H. Matsumura, T. Hayakawa, T. Ohta, Y. Nakashima, M. Miyamoto, T. C. Thi, K. Koyama, K. Ohdaira, *J. Appl. Phys.* **2014**, *116*, 114502.
[11] J. Seto, K. Ohdaira, H. Matsumura, *Jpn. J. Appl. Phys.* **2016**, *55*, 04ES05.
[12] M. Pomaska, W. Beyer, E. Neumann, F. Finger, K. Ding, *Thin Solid Films* **2015**, *595*, 217.
[13] K. Ohdaira, J. Seto, H. Matsumura, *Jpn. J. Appl. Phys.* **2017**, *56*, 08MB06.
[14] S. Tsuzaki, K. Ohdaira, T. Oikawa, K. Koyama, H. Matsumura, *Jpn. J. Appl. Phys.* **2015**, *54*, 072301.
[15] Y. Liu, D. Y. Kim, A. Lambertz, K. Ding, *Thin Solid Films* **2017**, *635*, 63.
[16] K. Ohdaira, T. T. Cham, H. Matsumura, *Jpn. J. Appl. Phys.* **2017**, *56*, 102301.
[17] W. E. Spear, P. G. Le Comber, *Solid State Commun.* **1975**, *17*, 1193.
[18] R. E. Hollingsworth, P. K. Bhat, *Appl. Phys. Lett.* **1994**, *64*, 616.
[19] F. Demichelis, C. F. Pirri, E. Tresso, *J. Appl. Phys.* **1992**, *72*, 1327.
[20] K. Wilken, F. Finger, V. Smirnov, *Energy Procedia* **2015**, *84*, 17.
[21] O. Astakhov, R. Carius, F. Finger, Y. Petrusenko, V. Borysenko, D. Barankov, *Phys. Rev. B* **2009**, *79*, 104205.
[22] T. Bronger, R. Carius, *Thin Solid Films* **2007**, *515*, 7486.
[23] R. Carius, F. Finger, U. Backhausen, M. Luysberg, P. Hapke, L. Houben, M. Otte, H. Overhof, in *Amorphous and Microcrystalline Silicon Technology - 1997*, Vol. *467* (Eds: S. Wagner, M. Hack, E. A. Schiff, R. Schropp, I. Shimizu), Materials Research Society, Warrendale, Pennsylvania **1997**, p. 283.
[24] A. Richter, F. Lentz, M. Meier, F. Finger, K. Ding, *Phys. Status Solidi A* **2016**, *213*, 1976.
[25] M. Köhler, M. Pomaska, F. Lentz, F. Finger, U. Rau, K. Ding, *ACS Appl. Mater. Interfaces* **2018**, *10*, 14259.

